bioRxiv preprint doi: https://doi.org/10.1101/2022.03.11.484052; this version posted March 12, 2022. The copyright holder for this preprint (which was not certified by peer review) is the author/funder, who has granted bioRxiv a license to display the preprint in perpetuity. It is made available under aCC-BY-NC-ND 4.0 International license.

1 # Visualization of mRNA Expression in *Pseudomonas aeruginosa* Aggregates
2 Reveals Spatial Patterns of Fermentative and Denitrifying Metabolism

3 Jadzia Livingston[1], Melanie A. Spero[1], Zachery R. Lonergan[1], Dianne K. Newman[1,2*]
4 [1]Division of Biology and Biological Engineering, Caltech, Pasadena, CA
5 [2]Division of Geological and Planetary Sciences, Caltech, Pasadena, CA
6 [*]corresponding author

7

8

9 **Abstract:**

10 Gaining insight into the behavior of bacteria at the single cell level is important given that
11 heterogeneous microenvironments strongly influence microbial physiology. The hybridization
12 chain reaction (HCR) is a technique that provides *in situ* molecular signal amplification, enabling
13 simultaneous mapping of multiple target RNAs at small spatial scales. To refine this method for
14 biofilm applications, we designed and validated new probes to visualize expression of key
15 catabolic genes in *Pseudomonas aeruginosa* aggregates. In addition to using existing probes for
16 the dissimilatory nitrate reductase (*narG*), we developed probes for a terminal oxidase (*ccoN1*),
17 nitrite reductase (*nirS*), nitrous oxide reductase (*nosZ*), and acetate kinase (*ackA*). These probes
18 can be used to determine gene expression levels both in liquid culture and in biofilms. Using
19 these probes, we quantified gene expression across oxygen gradients in aggregate populations
20 grown using the agar block biofilm assay (ABBA). We observed distinct patterns of catabolic
21 gene expression, with upregulation occurring in particular ABBA regions both within individual
22 aggregates and over the aggregate population. Aerobic respiration (*ccoN1*) showed peak
23 expression under oxic conditions, whereas fermentation (*ackA*) showed peak expression in the
24 anoxic cores of high metabolic activity aggregates near the air-agar interface. Denitrification
25 genes *narG, nirS,* and *nosZ* showed peak expression in hypoxic and anoxic regions, although *nirS*
26 expression was much stronger in anoxic environments compared to other denitrification genes.
27 These results reveal that the microenvironment correlates with catabolic gene expression in
28 aggregates, and demonstrate the utility of HCR in unveiling cellular activities at the microscale
29 in heterogeneous populations.

bioRxiv preprint doi: https://doi.org/10.1101/2022.03.11.484052; this version posted March 12, 2022. The copyright holder for this preprint (which was not certified by peer review) is the author/funder, who has granted bioRxiv a license to display the preprint in perpetuity. It is made available under aCC-BY-NC-ND 4.0 International license.

30

31 **Importance:**

32 To understand bacteria in diverse contexts we must understand the variations in behaviors and
33 metabolisms they express spatiotemporally. Populations of bacteria are known to be
34 heterogeneous, but the ways this variation manifests can be challenging to characterize due to
35 technical limitations. By focusing on energy conservation, we demonstrate that HCR v3.0 can
36 visualize nuances in gene expression, allowing us to understand how metabolism in
37 *Pseudomonas aeruginosa* biofilms responds to microenvironmental variation at high spatial
38 resolution. We validated probes for four catabolic genes: a constitutively expressed oxidase,
39 acetate kinase, nitrite reductase, and nitrous oxide reductase. We showed that the genes for
40 different modes of metabolism are expressed in overlapping but distinct subpopulations
41 according to oxygen concentrations in a predictable fashion. The spatial transcriptomic
42 technique described here has the potential to be used to map microbial activities across diverse
43 environments.

44

45 **Introduction:**

46 Even in an isogenic population, bacteria can display a range of different phenotypes
47 (Ackerman, 2015; Evans, 2020). This phenotypic variation can form along microenvironmental
48 gradients (Lara, 2006) but has also been observed in well-mixed cultures (Thattai, 2004; Kopf,
49 2015). Heterogeneity in gene expression allows cells to fit different ecological niches and
50 survive in ecosystems with fluctuating conditions, increasing the overall fitness of the
51 population (Thattai, 2004; Smits, 2006; Martins, 2015). Phenotypic heterogeneity is relevant in
52 a variety of contexts, from rhizosphere colonization (Broek, 2005) to metabolic engineering for
53 optimal biosynthesis of fuels and medicines (Xiao, 2016). In chronic infections, phenotypic
54 variation shields pathogens from antibiotics, allowing subpopulations with distinct metabolic
55 activities to survive rounds of treatment (Michiels, 2016; Fisher, 2017) and contribute to the
56 development of antibiotic resistance (Cohen, 2013).

57 While many technologies exist to study gene expression at the population (Guell, 2011)
58 and single cell (Kuchina, 2020) levels, few allow the mRNA output of individual bacteria to be

bioRxiv preprint doi: https://doi.org/10.1101/2022.03.11.484052; this version posted March 12, 2022. The copyright holder for this preprint (which was not certified by peer review) is the author/funder, who has granted bioRxiv a license to display the preprint in perpetuity. It is made available under aCC-BY-NC-ND 4.0 International license.

59 observed while maintaining the microenvironmental context and without genetically modifying
60 the cells (e.g. use of genetically-encoded fluorescent proteins). Recently, a spatial
61 transcriptomic method was introduced that enables visualization of hundreds of transcripts at a
62 time in single cells (Dar, 2021), yet this method requires specialized instrumentation and
63 analysis software, providing a barrier to widespread usage. By contrast, the hybridization chain
64 reaction (HCR) is a more accessible technology that permits single cell transcript visualization of
65 a smaller number of genes using standard instrumentation (Choi, 2018; Trivedi, 2018). HCR is a
66 form of fluorescence *in situ* hybridization (FISH), where the binding of fluorescent probes to a
67 target RNA of interest results in the binding of additional fluorescent probes, thus amplifying
68 the signal (Choi, 2018). The technology first was developed in eukaryotes (Dirks, 2004), but has
69 been used in bacteria to image rRNA for the purposes of species identification and growth rate
70 assessment in mixed communities (Nikolakakis, 2015; Depas, 2016), as well as to visualize gene
71 expression in heterogeneous populations (Jorth, 2020).
72 Building on these studies, we reasoned that HCR was well suited to enabling a
73 systematic exploration of the variation in catabolic activities within aggregate biofilms of the
74 model biofilm forming bacterium *Pseudomonas aeruginosa*. One environmental parameter that
75 has profound effects on the metabolic state of bacteria is oxygen. For example, many infection
76 sites have large regions of hypoxia, including those found in skin wounds, lungs, and the gut
77 (Palmer, 2007; Hong 2014), Additionally, opportunistic pathogens like *P. aeruginosa* can form
78 aggregate biofilms during infection, (Grant, 2013; Zhao, 2013; Depas, 2016), and biofilms
79 produce their own oxygen gradients, with biofilm-interior populations experiencing oxygen
80 limitation (Stewart, 2003). This has devastating consequences for human health because
81 commonly used antibiotics such as tobramycin and ciprofloxacin are ineffective at killing
82 oxygen-limited *P. aeruginosa* at the center of biofilms, while drugs that target anaerobic
83 metabolism specifically kill oxygen-limited populations (Walters, 2003; Spero, 2018).
84 Accordingly, antibiotic treatments must take the microenvironment and the phenotypic
85 heterogeneity experienced by opportunistic pathogens in the host into account to be successful
86 (Spiro, 2012; Cook, 2015). Before we can rationally design better treatments, we must improve

bioRxiv preprint doi: https://doi.org/10.1101/2022.03.11.484052; this version posted March 12, 2022. The copyright holder for this preprint (which was not certified by peer review) is the author/funder, who has granted bioRxiv a license to display the preprint in perpetuity. It is made available under aCC-BY-NC-ND 4.0 International license.

87 our understanding of the range of metabolic states that exist in biofilm populations
88 spatiotemporally (O'Toole, 2021).

89 In the absence of oxygen, *P. aeruginosa* cells utilize different strategies to conserve
90 energy, ranging from oxidative to substrate-level phosphorylation (Schobert, 2010). Because
91 chronic infections are often oxidant limited, how *P. aeruginosa* responds to electron acceptor
92 availability is expected to lead to metabolic differentiation within these environments, which
93 partly underpins its antibiotic tolerance and resistance (Ciofu, 2019). Under anoxic conditions,
94 *P. aeruginosa* can use nitrate and other N-oxides as alternative terminal electron acceptors to
95 oxygen by performing denitrification (Arat, 2015). The nitrate levels in chronic surgical wound
96 and cystic fibrosis lung infections are high enough to support denitrification in some regions,
97 while the oxygen levels are low enough to induce denitrification (Palmer, 2007; Line, 2014;
98 Turner, 2014). In the absence of nitrate, *P. aeruginosa* may survive under anoxic conditions for
99 long periods by performing pyruvate fermentation, in which pyruvate is converted to lactate
100 and acetate (Eschbach, 2004), or by fermenting arginine (Vander Wauven, 1984) or using
101 phenazines to facilitate glucose fermentation (Glasser, 2014). Aerobic, denitrifying, and
102 fermentative metabolisms are all relevant to bacterial populations in chronic infection
103 environments.

104 If we are to use HCR to map these metabolisms within biofilm aggregates, it is important
105 to interpret any gene expression patterns we might see within an ecophysiological regulatory
106 framework. In *P. aeruginosa,* the primary respiratory oxidase under highly aerobic conditions is
107 cbb_3-1, encoded by *cco1* (Jo, 2014). *cco1* is constitutively expressed when oxygen is replete but
108 slightly downregulated in stationary phase (Alvarez-Ortega, 2007; Arai, 2011). Denitrification is
109 catalyzed by a series of reductases, in particular *nar, nir, nor,* and *nos* (Arai, 2011; Arat, 2015).
110 The main regulatory proteins that govern the expression of these genes are Anr, Dnr, NarXL,
111 and NirQ (Figure 1). Under anoxic conditions, Anr activates Dnr, a regulatory protein that is
112 downregulated by phosphate availability, which activates NirQ. Where nitrate is available and
113 oxygen is limited, Anr additionally activates NarXL which in turn amplifies the activation of Dnr
114 and NirQ. The nitrate reductase gene, *nar*, is upregulated by NarXL, and this upregulation is
115 amplified by Dnr in the presence of nitric oxide (Arat, 2015). The nitrite reductase gene, *nir*, is

bioRxiv preprint doi: https://doi.org/10.1101/2022.03.11.484052; this version posted March 12, 2022. The copyright holder for this preprint (which was not certified by peer review) is the author/funder, who has granted bioRxiv a license to display the preprint in perpetuity. It is made available under aCC-BY-NC-ND 4.0 International license.

116 highly upregulated under anoxic conditions and has higher differential expression from oxic to
117 anoxic conditions than *nar* (Palmer, 2007; Alvarez-Ortega, 2007; Arai, 2011; Arat, 2015). *nir* is
118 slightly upregulated by Anr, causing a small amount of nitrite to be converted to nitric oxide,
119 which triggers Dnr and increases the upregulation of *nir* in a feedback loop (Kuroki, 2014). NirQ
120 and Dnr tightly coregulate *nir* with the nitric oxide reductase *nor* in response to nitric oxide
121 availability, preventing nitric oxide from accumulating (Arat, 2015). The nitrous oxide reductase,
122 *nos*, is upregulated by Dnr in response to nitric oxide availability (Arat, 2015). In contrast, the
123 acetate kinase gene, *ackA,* responsible for ATP synthesis during pyruvate and phenazine-
124 mediated glucose fermentation, is induced by the regulatory proteins Anr and IHF (Integration
125 host factor).

126 We targeted the expression levels of *cco1, narG*, *nirS*, *nosZ* and *ackA* mRNA molecules to
127 investigate the spatiometabolic patterning of catabolic gene expression within and across *P*.
128 *aeruginosa* aggregate biofilm populations. Our goal was to use a finite set of genes to identify
129 the range of metabolic states adopted by multicellular aggregates under oxidant-limited
130 conditions. Here we show that HCR 3.0 not only enables spatiometabolic mapping *in situ*, but
131 that it allows us to infer the metabolic state and environmental conditions that single cells
132 within these heterogeneous populations are experiencing.

133

134 **Results:**

135 **HCR Probes are Specific for their mRNA Targets**

136 To validate the probes designed for this study, we tested their specificity using WT and
137 mutant strains in which the target gene had been cleanly deleted. To test *narG* and *nirS* probes,
138 we grew WT, Δ*narGHJI*, and Δ*nirS* strains aerobically in LB supplemented with 40 mM nitrate to
139 late exponential phase to achieve oxygen limitation and activate Anr. To test *ccoN1* probes, we
140 grew WT and Δ*ccoN1* strains aerobically in the same medium to early exponential phase to
141 achieve highly oxygenated conditions. To test *nosZ* probes, we grew WT and Δ*nosZ* strains
142 anaerobically in the same medium to mid-exponential phase to achieve denitrifying
143 metabolism. We were unable to observe *ackA* signal in any of the liquid culture conditions we
144 tested, so to test *ackA* probes, WT and Δ*ackA* were grown in the agar biofilm block assay

bioRxiv preprint doi: https://doi.org/10.1101/2022.03.11.484052; this version posted March 12, 2022. The copyright holder for this preprint (which was not certified by peer review) is the author/funder, who has granted bioRxiv a license to display the preprint in perpetuity. It is made available under aCC-BY-NC-ND 4.0 International license.

145 (ABBA) for 12 hours in LB medium and 0.5% agar, supplemented with 40 mM nitrate. Briefly, in
146 ABBA, *P. aeruginosa* cells are suspended in an agar medium that is allowed to solidify. Cells
147 then grow as aggregate biofilms suspended in this agar matrix, and nutrient gradients are
148 known to develop within individual aggregates as well as across the population of aggregates
149 (see below).

150 The *narG*, *nirS*, *nosZ*, *and ccoN1* probes showed an average mean intensity per cell that
151 was an order of magnitude higher in the wildtype compared to the deletion strains, indicating
152 our probe sets are specific for each target mRNA (Figures 2A, 2C). Additionally, the *ackA* probe
153 showed significantly higher average mean intensity per ABBA aggregate compared to the
154 deletion strain (Figures 2B, 2D). In some of the deletion mutant controls, particularly for the
155 *nosZ* and *ccoN1* probe sets, we occasionally observed fluorescent puncta that did not overlap
156 with cells and appeared qualitatively different from the signal observed in the positive control.
157 We therefore assume that these puncta were due to non-specific binding to the slide and not
158 biologically significant.
159

160 **Metabolite Gradients are Readily Established in ABBA**

161 To explore the phenotypic heterogeneity of *P. aeruginosa* wildtype PA14, we used HCR
162 to visualize the localization of *narG*, *nirS*, *nosZ*, *ccoN1*, and *ackA* expression across biofilm
163 aggregates grown in the ABBA. Within ABBAs, cells generate oxygen and nitrate gradients over
164 the course of a few hours. We used a thresholded 16S rRNA intensity value to define aggregate
165 boundaries and to control for baseline metabolic activity, and quantified mRNA and rRNA
166 signals within this mask. *P. aeruginosa* aggregates were grown in LB medium with 0.5% agar,
167 supplemented with 40 mM nitrate. We chose these conditions to capture the effects of oxygen
168 and nitrate gradients on the expression of our genes of interest. Physiological levels of nitrate in
169 infected cystic fibrosis lung samples and chronic wounds are ~400 μM (Palmer, 2007;
170 Bernatchez, 2013), but we chose a higher concentration of nitrate to ensure that it would still
171 be available after 12 hours of growth.

172 In an ABBA, an oxygen gradient develops, and the oxygen minimum migrates upwards
173 towards the air-agar interface over the course of the incubation as cell density increases, and

bioRxiv preprint doi: https://doi.org/10.1101/2022.03.11.484052; this version posted March 12, 2022. The copyright holder for this preprint (which was not certified by peer review) is the author/funder, who has granted bioRxiv a license to display the preprint in perpetuity. It is made available under aCC-BY-NC-ND 4.0 International license.

174 thus oxygen availability decreases (Figure 3A). The exact depths at which oxygen is minimal vary
175 between agar blocks, but the pattern is conserved. A steep oxygen gradient occurs across the
176 first ~100 microns directly below the surface, and regions deeper than ~250 μm are uniformly
177 oxygen starved. Accordingly, deeper aggregates in the anoxic zone will have experienced anoxia
178 for longer than the aggregates above them. As aggregates begin experiencing hypoxia, cells will
179 upregulate denitrification genes and reduce nitrate, such that a similar nitrate gradient is also
180 expected to develop. The deepest aggregates are likely the first to begin consuming nitrate in
181 their local environment, so deeper aggregates likely have less access to nitrate at this time
182 point. As the denitrification pathway proceeds, nitric oxide is generated (Williams, 1978), so a
183 greater amount of nitric oxide is expected at lower depths.

184 Given these conditions and the regulatory architecture controlling expression of these
185 genes (Figure 1), we predicted that *narG* would be expressed in regions with high nitrate and
186 low oxygen concentrations, *nirS* would be expressed in regions with high nitrate and/or nitric
187 oxide and low oxygen concentrations, and *nosZ* would be expressed in regions with nitric oxide
188 present and low oxygen concentrations. We expected *ccoN1* to be expressed most highly in
189 regions with high oxygen and *ackA* to be expressed in regions that are limited for both oxygen
190 and nitrate.

191

192 **Metabolic Genes Show Distinct Expression Patterns within ABBAs**

193 The oxidase *ccoN1* was maximally expressed in the oxic region (0-50 μm from the air-
194 agar interface at the top of the ABBA blocks), and steeply decreased in expression deeper into
195 the block along the oxygen gradient which is the same pattern shown by the 16S rRNA signal
196 (Figure 3B). In the larger aggregates closer to the surface, signal for *ccoN1* and 16S rRNA was
197 higher along the aggregate exterior than in the centers, while signal for the *ackA* gene was
198 highly expressed in the interior (Figures 3B,3C, Figure S1). Elevated signal for the denitrification
199 genes was not detected in this region.

200 In the region below the oxic portion of our experimental system (>50 μm from the air-
201 agar interface at the top of the ABBA blocks), rRNA, *ccoN1* and *ackA* expression was reduced,
202 and expression of the denitrification genes were elevated, correlating with low oxygen

bioRxiv preprint doi: https://doi.org/10.1101/2022.03.11.484052; this version posted March 12, 2022. The copyright holder for this preprint (which was not certified by peer review) is the author/funder, who has granted bioRxiv a license to display the preprint in perpetuity. It is made available under aCC-BY-NC-ND 4.0 International license.

203 concentrations that decreased with depth across this region (Figure 3A, 3B, 3C) All three
204 denitrification genes were expressed at their maximal levels in aggregates in this region. The
205 nitrate reductase *narG* was upregulated under hypoxic conditions in the 40 mM nitrate
206 samples, peaking in average mean intensity per aggregate at a depth of 100-150 μm from the
207 air-agar interface (Figure 3B, 3C). *narG* signal was restricted to the interior of aggregates,
208 where oxygen availability is expected to be reduced compared to cells on the aggregate
209 exterior (Figure 3B, Figure S1). The nitrite reductase *nirS* was upregulated under hypoxic and
210 anoxic conditions, peaking between 100-200 μm from the surface. The nitrous oxide reductase
211 *nosZ* was expressed in cells in the cores of some aggregates in the hypoxic and anoxic regions,
212 but was not uniformly expressed by aggregates at any depth (Figure 3C). Oxygen levels reached
213 their minimal levels between 150-250 μm from the air-agar interface (Figure 3A).
214 Oxygen levels were uniformly low below 250 μm from the air-agar interface. All genes
215 measured showed reduced expression with depth across this anoxic region, likely due to
216 oxidant limitation, although *nirS* expression was elevated in the cores of aggregates at all
217 depths. *nirS* signal was restricted to the interior of aggregates in the hypoxic zone, but was
218 expressed across entire aggregates further into the anoxic zone (Figure 3B, Figure S1).
219 Appreciable *narG* signal was not detected in the deepest anoxic region (Figure 3C). Data from
220 two additional replicates of this experiment (mRNA and rRNA ABBA images with quantification)
221 can be found in Figures S2-S7.
222
223 **Differentially Regulated Metabolic Genes show Different Expression Patterns than rRNA**
224 By comparing the rRNA and mRNA signal per aggregate in each sample, we can detect
225 where the mRNA signal diverges from the basal metabolic rate, reflected by the rRNA signal.
226 The *ccoN1* signal linearly and positively covaried with the rRNA signal across depths (Figure 4).
227 No other genes showed this pattern. All three denitrification genes showed maximal expression
228 in regions where the rRNA signal was ≤ half the maximum, corresponding to the hypoxic
229 transition region of the agar block. The *nirS* signal showed the highest negative covariance with
230 the rRNA signal, with maximal expression occurring in aggregates with one-third the maximum
231 rRNA signal. The *ackA* signal showed positive, but non-linear, covariance with the rRNA signal,

bioRxiv preprint doi: https://doi.org/10.1101/2022.03.11.484052; this version posted March 12, 2022. The copyright holder for this preprint (which was not certified by peer review) is the author/funder, who has granted bioRxiv a license to display the preprint in perpetuity. It is made available under aCC-BY-NC-ND 4.0 International license.

232 showing the highest mRNA signal in the aggregates at the surface with the highest rRNA signal,
233 and linearly covarying throughout the oxic and hypoxic regions before a steep dropoff of mRNA
234 signal in the anoxic region. The rRNA and *ccoN1* signals were qualitatively highest at the
235 aggregate edges, while the *narG*, *nirS*, and *nosZ* signals were highest in the aggregate cores
236 (Figure S1), likely indicating a radial oxygen gradient from the edges to the cores of individual
237 aggregates. The *ackA* signal was heterogeneously expressed in some cells throughout
238 aggregates.
239
240 **Discussion:**
241 In this work, we developed and validated a set of HCR probes targeting *mRNA* molecules
242 for key denitrification, aerobic respiration, and fermentation genes in *P. aeruginosa.* This
243 targeted probe set permits mapping of the metabolic states of cells in aggregate biofilms at
244 high resolution across microenvironments characterized by steep oxygen and nitrate gradients.
245 Our results reveal distinct patterns of catabolic gene expression within these populations,
246 underscoring that metabolic activity can be heterogeneous over small spatial scales. The
247 demonstration that HCR can be applied to chart catabolism within a reductionist laboratory
248 biofilm sets the stage for future studies of microbial responses to dynamic microenvironments
249 in more complex contexts. Importantly, HCR permits the study of gene expression dynamics in
250 complex wildtype populations without the need for generating reporter strains; though
251 developed here for a model organism, this capability has obvious advantages for the study of
252 strains that are not yet genetically tractable.
253 Our results show that the relationship between *ccoN1* and rRNA signals for entire
254 aggregates is linear and positive, indicating that changes in *ccoN1* expression reflect changes in
255 the metabolic rate on the population level (DePas, 2016). This is consistent with previous
256 studies showing *ccoN1* as constitutively expressed (Jo, 2017). Most genes in Gram-negative
257 bacteria such as *P. aeruginosa* show basal levels of gene expression even outside the
258 upregulation condition (Volke, 2020) so the expression pattern shown by *ccoN1* represents the
259 null hypothesis of what expression should look like if the gene is not regulated by
260 environmental conditions. If gene expression patterns diverge from the pattern shown by

bioRxiv preprint doi: https://doi.org/10.1101/2022.03.11.484052; this version posted March 12, 2022. The copyright holder for this preprint (which was not certified by peer review) is the author/funder, who has granted bioRxiv a license to display the preprint in perpetuity. It is made available under aCC-BY-NC-ND 4.0 International license.

261 *ccoN1* and rRNA, we can infer that they are upregulated and downregulated based on
262 additional conditions other than the metabolic rate.

263 We observed that expression of the genes encoding the denitrification machinery in *P.*
264 *aeruginosa* is spatially stratified across the ABBA system after 12 hours. Previous studies have
265 demonstrated that denitrification in liquid cultures occurs in successive steps over time
266 (Williams, 1978). Recently this sequential pattern was observed in structured communities of *P.*
267 *aeruginosa* for *narG* and *nirS* using reporter strains (Smirga, 2021), revealing maximal
268 expression of these genes moved outward from the center of particles suspended in bulk
269 medium across time, suggesting aggregates progressively extinguished local oxygen, nitrate,
270 and nitric oxide concentrations. Our findings confirm this spatial pattern in *P. aeruginosa*,
271 showing that at a single time point maximal *narG* expression occurs closer to the air-agar
272 interface than maximal *nirS* and *nosZ* expression, as oxygen limitation and nitrate limitation
273 increase with depth. Furthermore, we were able to visualize this spatial pattern in individual
274 aggregates. In aggregates between 50-150 μm from the air-agar interface, *narG* expression
275 occurs closer to the exterior of individual aggregates compared to *nirS* and *nosZ* expression, and
276 *nirS* expression is present across entire aggregates at greater, mostly anoxic depths but limited
277 to the cores of aggregates in hypoxic conditions.

278 Despite both being upregulated by Anr, fermentation and denitrification genes showed
279 distinct expression patterns. The fermentation gene *ackA* was upregulated in the cores of the
280 aggregates closest to the air-agar interface where oxygen concentrations are higher, while the
281 denitrification genes were upregulated in the cores of the aggregates in the hypoxic regions.
282 Both types of metabolism mark hypoxic/anoxic conditions, but they are regulated in response
283 to distinct nitrate and nitric oxide conditions. Given that *ackA* is expressed in the absence of
284 nitrate (Eschbach, 2004), the pattern of the denitrification and fermentation genes suggests
285 that the cores of the aggregates at the top of the agar blocks may be conserving energy by
286 fermentation, due to a microenvironmental regulatory cue. Notably, the denitrification genes
287 are directly upregulated by Dnr, which is activated by nitric oxide, while *ackA* is directly
288 upregulated by Anr, which is deactivated by nitric oxide. We can infer from this regulatory
289 relationship that nitric oxide signaling is occurring in the lower aggregates but not in the upper

bioRxiv preprint doi: https://doi.org/10.1101/2022.03.11.484052; this version posted March 12, 2022. The copyright holder for this preprint (which was not certified by peer review) is the author/funder, who has granted bioRxiv a license to display the preprint in perpetuity. It is made available under aCC-BY-NC-ND 4.0 International license.

290 aggregates at this time point. Direct measurement of N-oxide concentrations in the ABBA
291 system is important for understanding the relationship between microenvironmental
292 conditions and metabolic state, and will be the focus of future experiments.
293 Going forward, this set of probes may be expanded and multiple high-signal probes may
294 be used to determine correlation and anticorrelation more precisely. HCR may be used in two
295 directions: read-out, in which specific regions of a sample are queried to learn which genes are
296 co-expressed within them, and read-in, in which knowledge of genes whose co-expression is
297 already understood is leveraged to infer something about the microenvironment of the region
298 in which they are expressed (Trivedi, 2018). The former application allows us to choose a
299 specific context in space and time and see which genes are being expressed without prior
300 knowledge, whereas the latter approach allows us to apply our knowledge of gene regulation to
301 infer something about the microenvironment–such as we did in this study to dissect the
302 microenvironmental conditions of ABBA subpopulations. In the future, the probes developed in
303 this study may be applied to observe metabolisms and infer potential microenvironmental
304 conditions experienced by *P. aeruginosa* in clinical samples, opening the doors for greater
305 insight into the metabolic processes sustaining cells in infections.
306
307 **Acknowledgements:**
308
309 We thank Lars Dietrich and Lindsey Christine Florek for the Δ*ccoN1* PA14 strain, Steven Wilbert for the
310 Δ*nirS* and Δ*nosZ* strains, and David Basta and Nate Glasser for the Δ*ackA* strain. We thank Chelsey
311 VanDrisse, Steven Wilbert, John Ciemnieki and Georgia Squyres for constructive feedback and we thank
312 Niles Pierce, and Maayan Schwarzkopf for assistance using the HCR system. Confocal microscopy was
313 performed in the Caltech Biological Imaging Facility at the Caltech Beckman Institute, which is supported
314 by the Arnold and Mabel Beckman Foundation, and we thank Giada Spigolon for her help using the
315 facility. This work was supported by grants from the NIH (R01 HL152190-03) to DKN, the Doren Family
316 Foundation, the Cystic Fibrosis Foundation (postdoctoral fellowship to MAS, SPERO19F0), and the Jane
317 Coffin Childs Memorial Fund (postdoctoral fellowship to ZRL).
318
319

bioRxiv preprint doi: https://doi.org/10.1101/2022.03.11.484052; this version posted March 12, 2022. The copyright holder for this preprint (which was not certified by peer review) is the author/funder, who has granted bioRxiv a license to display the preprint in perpetuity. It is made available under aCC-BY-NC-ND 4.0 International license.

320 **Materials and Methods:**

321

322 **Microbial strains and growth conditions**

323 *P. aeruginosa* strains UCBPP- PA14 (wild type (WT)) and isogenic Δ*narGHJI* (Spero, 2018), Δ*ccoN1* (Jo,
324 2017), Δ*ackA* (Glasser, 2014), Δ*nirS* and Δ*nosZ* (Wilbert, 2021) were routinely grown in 5 mL Luria
325 Bertani (LB) broth supplemented with 40 mM KNO3 shaking at 37°C. Aerobic cultures were incubated at
326 37°C shaking at 250 rpm unless described otherwise. Anaerobic cultures were incubated in an anaerobic
327 chamber at 37°C without shaking.

328

329 **HCR v3.0 probe validation**

330 WT and deletion mutant cultures were grown overnight from freezer stocks in LB broth supplemented
331 with 40 mM KNO3. For the *ackA* mutant, cells were grown in the agarose biofilm block assay (ABBA) as
332 described below. For other mutants, 20 μL overnight culture was inoculated into 5 mL of pre-warmed
333 and degassed media and incubated under conditions meant to induce upregulation of the target gene.
334 For *narG* and *nirS*, cultures were grown aerobically as described above for 4 hours to an approximate
335 optical density at 500 nm of 1.1. For *ccoN1,* cultures were grown aerobically as described above for 2.5
336 hours to an approximate optical density at 500 nm of 0.2. For *nosZ,* wildtype and deletion mutant
337 cultures were grown anaerobically for 2.5 hours, to an approximate optical density at 500 nm of 0.2. 1
338 mL of culture was pelleted and cells were fixed by resuspending in 1 mL of 4% paraformaldehyde in
339 phosphate-buffered saline (PBS) pH 7.2, and incubating resuspensions at 25°C for 90 minutes. After
340 fixing, cells were pelleted, washed with PBS, resuspended in 1mL of a 1:1 ethanol:PBS solution, and
341 stored at -20C until HCR 3.0 experiments were performed.

342

343 Prior to performing HCR, cell suspensions were washed in PBS and treated with 1 mg/ml lysozyme
344 (catalog number L6876; Sigma) in 10 mM Tris-HCl (pH 7.6) for 1 h at 37°C with shaking. After these
345 treatments, cells were washed with PBS, resuspended in 1mL of a 1:1 ethanol:PBS solution. Cell
346 solutions were suspended in hybridization buffer for 1 hour at 37˚C. Probe solutions were prepared,
347 containing 5 nM of appropriate HCR v3.0 initiator odd and even probe pairs in filter-sterilized
348 hybridization buffer. 20 uL of probe solutions (Integrated DNA Technologies) were added to each cell
349 solution. *Pseudomonas aeruginosa* rRNA and *narG* mRNA sequences were targeted using target
350 sequences previously used in Jorth, 2020. Probes specific to *nirS*, *nosZ*, *ackA*, and *ccoN1* were designed
351 in the study, and the target sequences are included in Table S1. Solutions were hybridized overnight at

bioRxiv preprint doi: https://doi.org/10.1101/2022.03.11.484052; this version posted March 12, 2022. The copyright holder for this preprint (which was not certified by peer review) is the author/funder, who has granted bioRxiv a license to display the preprint in perpetuity. It is made available under aCC-BY-NC-ND 4.0 International license.

352 37˚C, then washed twice with 200 uL probe wash buffer at 37˚C. Cells were then resuspended in 40 μL
353 amplification buffer and pre-amplified for 30 minutes, while fluorescent hairpin probes (Molecular
354 Technologies) were thawed, each denatured in separate tubes in a thermal cycler for 90s at 95°C and
355 allowed to cool for at least 30 m at 25°C in the dark.
356
357 Hairpins with Alexa Fluor 488 were used for the rRNA probes, and hairpins with Alexa Fluor 647 were
358 used for the mRNA probes. The B1 initiator/hairpin system from Molecular Technologies was used for
359 rRNA, while B2 was used for *nosZ* and *ccoN1* mRNA, B3 was used for *narG* mRNA, and B4 was used for
360 *nirS* and *ackA* mRNA. 25 uL of each hairpin were suspended in 20 uL of amplification buffer and added to
361 the cell solutions, and incubated overnight in the dark at 25˚C. The cells were then washed three times
362 in 200 uL 5X SSCT, before being resuspended in 20 uL 5X SSCT and spotted onto a microscope slide
363 (catalog number: 3039-002; ThermoFisher) and allowing to dry overnight in the dark at 4˚C. Finally,
364 slides were washed with ice-cold ~0°C ultra-purified water, then with -20°C ethanol, and slides were
365 allowed to air-dry at 25°C in the dark. Each dried cell spot was then covered with 2.5 ml ProLong Gold
366 Antifade Mountant (catalog number: P36930; ThermoFisher), slides were incubated for 48 hours in the
367 dark at 25°C before being stored, and imaged using a Nikon Eclipse Ti2 fluorescence microscope at 40x
368 magnification with 50% laser power and 1 second exposure for the fluorescent channels. Image analysis
369 was performed using FIJI. Phase images were thresholded to produce a mask and detect cells, then the
370 marked cells were thresholded by rRNA signal to eliminate non-bacterial debris from the dataset, then
371 mean intensity was determined for each labeled cell. Quantitative graphs were generated using bokeh.
372
373 Hybridization, probe wash, and amplification buffers were acquired from Molecular Technologies
374 (Caltech, Pasadena, CA).
375
376 **ABBA Preparation:**
377 ABBA samples were prepared as described previously (Jorth, 2020). Two sequential overnight cultures of
378 wildtype *P. aeruginosa* PA14 were grown in the same liquid media as the final ABBAs, shaking
379 aerobically at 37˚C, then diluted to OD_{500} .001 in molten LB supplemented with nitrate depending on
380 experimental conditions and 0.5% noble agar. The agar suspension was transferred to chambered cover
381 glass slides and allowed to cool for 10 minutes, before being transferred to a humidified chamber and
382 incubated at 37˚C for 12 hours. After 12 hours, blocks were carefully removed from their chambers
383 using a sterilized metal spatula into pre-chilled 1 mL of 4% paraformaldehyde in PBS + ProtectRNA and

bioRxiv preprint doi: https://doi.org/10.1101/2022.03.11.484052; this version posted March 12, 2022. The copyright holder for this preprint (which was not certified by peer review) is the author/funder, who has granted bioRxiv a license to display the preprint in perpetuity. It is made available under aCC-BY-NC-ND 4.0 International license.

384 incubated for 24 hours at 4˚C. Blocks were washed three times for 30 minutes each in 1 mL PBS, then
385 incubated for 1 hour in 1 mg/mL lysozyme in 10 mM Tris HCl at 37˚C to lyse cell walls, then washed
386 again three times for 30 minutes each in 1 mL PBS and stored in 1 mL PBS. Blocks were checked on a
387 microscope for proper growth patterning (large aggregates at the top and smaller ones in the bottom,
388 for wildtype in LB+40 mM nitrate) prior to continuing. For each condition and each gene target, three
389 biological replicates were performed, in addition to one blank (no cell inoculation) per condition.
390
391 **ABBA HCR:**
392 For each sample, 500 μL of hybridization buffer was mixed with 1 μL even and odd HCR initiator probes
393 (2 μM stock) for 4 nM ultimate concentration. Each block was incubated in the buffer overnight at 37˚C,
394 then washed three times for 2 hours in the 1 ml pre-warmed wash buffer at 37˚C. Each sample was then
395 combined with 250 μL of preheated amplification buffer and 5 μL snap-cooled fluorescent hairpins (3
396 μM stock) for 60 nM final concentration. Samples were incubated overnight in the dark at room
397 temperature, then washed for 6 hours in 1 mL 5X SSCT at room temperature in the dark, then
398 transferred to 500 ul PBS and stored at 4˚C in the dark until imaging using confocal fluorescence
399 microscopy. Imaging was performed on a Zeiss LSM 800 in the Caltech Bioimaging Facility. Agar blocks
400 were mounted on a glass-bottomed dish with the original air-agar interface oriented toward the glass
401 bottom. Both the Alexa Fluor 488 rRNA and Alexa Fluor 647 mRNA channels were imaged
402 simultaneously, with a laser power of .2% and a gain of 650 for the 488 channel, and a laser power of 2%
403 and a gain of 750 for the 647 channel. At least four image fields were imaged per sample using a 10x
404 objective with 2x zoom, for a final image field of 319.45 x 319.45 microns. For each image field, a 100
405 slice z-stack was imaged with an interslice distance of 6.24 microns. Images were framed such that the
406 surface, which appears visible as a plane of rRNA signal due to a lawn of cells growing on the agar
407 surface, was within 4 slices of the top of the image. Quantification of fluorescence signal per aggregate
408 was performed using Imaris v9.5.1. A batch pipeline was created to segment aggregates. The 488 signal
409 intensity of each Z plane was normalized, and then aggregates were segmented based on the
410 thresholded 488 signal, with the threshold chosen manually per imaging date. The normalized signal was
411 only used for the purpose of segmentation, and the mean signal intensity values reported here are
412 based on the raw signal rather than the normalized signal. The mean 488 and 647 mRNA signal intensity,
413 as well as aggregate size, was calculated and exported per aggregate. Depth was defined as distance
414 from the top of the image, and images were cropped for analysis such that the surface was at the top

bioRxiv preprint doi: https://doi.org/10.1101/2022.03.11.484052; this version posted March 12, 2022. The copyright holder for this preprint (which was not certified by peer review) is the author/funder, who has granted bioRxiv a license to display the preprint in perpetuity. It is made available under aCC-BY-NC-ND 4.0 International license.

415 slice using native Imaris functions. Quantitative graphs were generated using seaborn and bokeh. Raw
416 images were displayed using FIJI.
417

bioRxiv preprint doi: https://doi.org/10.1101/2022.03.11.484052; this version posted March 12, 2022. The copyright holder for this preprint (which was not certified by peer review) is the author/funder, who has granted bioRxiv a license to display the preprint in perpetuity. It is made available under aCC-BY-NC-ND 4.0 International license.

418 **Figure Legends**

419 **Figure 1: Regulatory Diagram of Target Genes** This diagram was compiled from a literature
420 search of transcriptomics reviews in *P. aeruginosa*. (Eschbach, 2004; Arai, 2005; Schreiber,
421 2007; Arai, 2011; Arat, 2015)

422 **Figure 2: mRNA Probes Are Target-Specific** (A) Micrographs of Single Cell Deletion Validation
423 Controls for mRNA Probes. (B) Micrographs of Aggregate Deletion Validation Controls for mRNA
424 probes. Images reflect the region 50-100 µm from the air-agar interface. (C) Quantification of
425 mean mRNA probe intensities for single cells grown in liquid culture of wildtype and deletion
426 mutants for target genes under upregulating growth conditions. Mean intensity was 10-fold
427 higher in the wildtype than in the deletion for all probe sets. Each boxplot summarizes
428 approximately 10 images per replicate. Three replicates were performed per condition. (D)
429 Quantification of mean mRNA probe intensities for aggregates grown in agar blocks wildtype
430 and deletion mutants for *ackA* under upregulating growth conditions. Mean intensity was 2-
431 fold higher in the wildtype, and each boxplot summarizes 3-5 images per replicate. Three
432 replicates were performed per condition.

433 **Figure 3: Metabolic Genes Show Distinct Patterns Across 3D Oxygen Gradients (**A) Mean
434 oxygen levels of ABBA samples grown with LB+40 mM Nitrate for 12 hours. The dark line is the
435 mean, while the shading represents the standard deviation of 8 biological replicates grown
436 under identical conditions. (B) 3D Micrographs of Probe Signal in LB + 40 mM Nitrate ABBAs.
437 Each image represents a 50 micron slice of agar, compiled from 8 individual z-slices with an
438 interslice distance of 6.24 microns, viewed from the top of the block, with each sequential
439 image from the top of the figure representing the section directly below the slice above it. rRNA
440 signal is colored cyan, while mRNA signal is colored magenta. (C) Mean mRNA Channel Intensity
441 per aggregate (x axis) plotted by depth. Each plot represents four images of one replicate each
442 of an experimental and control condition, and each point represents one aggregate. Filled
443 points represent the experimental condition, while the white circles represent a control
444 condition where only rRNA probes were used.

445 **Figure 4: Metabolic Genes Show Distinct Patterns Compared to rRNA Expression** Mean mRNA
446 intensity per aggregate (x) plotted against mean rRNA intensity per aggregate (y) colored by

bioRxiv preprint doi: https://doi.org/10.1101/2022.03.11.484052; this version posted March 12, 2022. The copyright holder for this preprint (which was not certified by peer review) is the author/funder, who has granted bioRxiv a license to display the preprint in perpetuity. It is made available under aCC-BY-NC-ND 4.0 International license.

447 depth. Each plot represents four z-stacks of one replicate, and each point represents one
448 aggregate. Large points represent the experimental condition, and small points represent the
449 control condition without mRNA probes.
450
451

bioRxiv preprint doi: https://doi.org/10.1101/2022.03.11.484052; this version posted March 12, 2022. The copyright holder for this preprint (which was not certified by peer review) is the author/funder, who has granted bioRxiv a license to display the preprint in perpetuity. It is made available under aCC-BY-NC-ND 4.0 International license.

452 **Bibliography:**

453 Ackermann, M. (2015). A functional perspective on phenotypic heterogeneity in
454 microorganisms. Nature Reviews. Microbiology, 13(8), 497–508.
455 https://doi.org/10.1038/NRMICRO3491
456 Arai, H. (2011). Regulation and function of versatile aerobic and anaerobic respiratory
457 metabolism in *Pseudomonas aeruginosa*. Frontiers in Microbiology, 2(MAY), 103.
458 https://doi.org/10.3389/fmicb.2011.00103
459 Arat, S., Bullerjahn, G. S., & Laubenbacher, R. (2015). A network biology approach to
460 denitrification in *Pseudomonas aeruginosa*. PLOS ONE, 10(2), e0118235.
461 https://doi.org/10.1371/journal.pone.0118235
462 Bernatchez, S. F., Menon, V., Stoffel, J., Walters, S. A. H., Lindroos, W. E., Crossland, M.
463 C., … Boykin, J. V. (2013). Nitric oxide levels in wound fluid may reflect the healing
464 trajectory. Wound Repair and Regeneration, 21(3), 410–417.
465 https://doi.org/10.1111/WRR.12048
466 Bernhard, A. (2010). The Nitrogen Cycle: Processes, Players, and Human Impact. Nature.
467 Retrieved from https://www.nature.com/scitable/knowledge/library/the-nitrogen-
468 cycle-processes-players-and-human-15644632/
469 Broek, D. Van Den, Bloemberg, G. V., & Lugtenberg, B. (2005). The role of phenotypic
470 variation in rhizosphere *Pseudomonas* bacteria. Environmental Microbiology, 7(11),
471 1686–1697. https://doi.org/10.1111/J.1462-2920.2005.00912.X
472 Chen, Z., Chen, L., & Zhang, W. (2017). Tools for genomic and transcriptomic analysis of
473 microbes at single-cell level. Frontiers in Microbiology, 8(SEP), 1831.
474 https://doi.org/10.3389/FMICB.2017.01831
475 Choi, H. M. T. T., Beck, V. A., & Pierce, N. A. (2014). Next-generation in situ hybridization
476 chain reaction : higher gain , lower cost , greater durability. ACS Nano, 8(5), 4284–
477 4294. https://doi.org/10.1021/nn405717p
478 Choi, H. M. T., Schwarzkopf, M., Fornace, M. E., Acharya, A., Artavanis, G., Stegmaier, J., …
479 Pierce, N. A. (2018). Third-generation in situ hybridization chain reaction: multiplexed,

bioRxiv preprint doi: https://doi.org/10.1101/2022.03.11.484052; this version posted March 12, 2022. The copyright holder for this preprint (which was not certified by peer review) is the author/funder, who has granted bioRxiv a license to display the preprint in perpetuity. It is made available under aCC-BY-NC-ND 4.0 International license.

480 quantitative, sensitive, versatile, robust. Development (Cambridge), 1(12), 285213.
481 https://doi.org/10.1242/dev.165753
482 Cohen, N., MA, L., & JJ, C. (2013). Microbial persistence and the road to drug resistance.
483 Cell Host & Microbe, 13(6), 632–642. https://doi.org/10.1016/J.CHOM.2013.05.009
484 Cook, G. M., Greening, C., Hards, K., & Berney, M. (2014). Energetics of pathogenic
485 bacteria and opportunities for drug development. Advances in Microbial Physiology
486 (1st ed., Vol. 65). Elsevier Ltd. https://doi.org/10.1016/bs.ampbs.2014.08.001
487 Cowley, E. S., Kopf, S. H., Lariviere, A., Ziebis, W., & Newman, D. K. (2015). Pediatric cystic
488 fibrosis sputum can be chemically dynamic, anoxic, and extremely reduced due to
489 hydrogen sulfide formation. MBio, 6(4), 1–15. https://doi.org/10.1128/mBio.00767-
490 15
491 Dar, D., Dar, N., Cai, L., & Newman, D. K. (2021). Spatial transcriptomics of planktonic and
492 sessile bacterial populations at single-cell resolution. Science (New York, N.Y.),
493 373(6556). https://doi.org/10.1126/SCIENCE.ABI4882
494 Delic-Attree, I., B, T., A, F., JC, W., & PM, V. (1996). Isolation of an IHF-deficient mutant of a
495 *Pseudomonas aeruginosa* mucoid isolate and evaluation of the role of IHF in algD
496 gene expression. Microbiology (Reading, England), 142 (Pt 1(10), 2785–2793.
497 https://doi.org/10.1099/13500872-142-10-2785
498 DePas, W., Starwalt-Lee, R., Sambeek, L., Kumar, S., Gradinaru, V., & Newman, D. (2016).
499 Exposing the three-dimensional biogeography and metabolic states of pathogens in
500 cystic fibrosis sputum via hydrogel embedding, clearing, and rRNA labeling. Mbio,
501 7(5), e00796-16. https://doi.org/10.1128/mBio.00796-16
502 Dirks, R. M., & Pierce, N. A. (2004). From the Cover: Triggered amplification by
503 hybridization chain reaction. Proceedings of the National Academy of Sciences of the
504 United States of America, 101(43), 15275. https://doi.org/10.1073/PNAS.0407024101
505 Eschbach, M., K, S., K, T., J, B., D, J., & M, S. (2004). Long-term anaerobic survival of the
506 opportunistic pathogen *Pseudomonas aeruginosa* via pyruvate fermentation. Journal
507 of Bacteriology, 186(14), 4596–4604. https://doi.org/10.1128/JB.186.14.4596-
508 4604.2004

bioRxiv preprint doi: https://doi.org/10.1101/2022.03.11.484052; this version posted March 12, 2022. The copyright holder for this preprint (which was not certified by peer review) is the author/funder, who has granted bioRxiv a license to display the preprint in perpetuity. It is made available under aCC-BY-NC-ND 4.0 International license.

509 Evans, T. D., & Zhang, F. (2020). Bacterial metabolic heterogeneity: origins and applications
510 in engineering and infectious disease. Current Opinion in Biotechnology, 64, 183–189.
511 https://doi.org/10.1016/J.COPBIO.2020.04.007
512 Fei, J., & Sharma, C. M. (2018). RNA localization in bacteria. Microbiology Spectrum, 6(5).
513 https://doi.org/10.1128/microbiolspec.rwr-0024-2018
514 Fisher, R. A., Gollan, B., & Helaine, S. (2017). Persistent bacterial infections and persister
515 cells. Nature Reviews Microbiology 2017 15:8, 15(8), 453–464.
516 https://doi.org/10.1038/nrmicro.2017.42
517 Galán-Vásquez, E., Luna, B., & Martínez-Antonio, A. (2011). The regulatory network of
518 *Pseudomonas aeruginosa*. Microbial Informatics and Experimentation, 1(1), 3.
519 https://doi.org/10.1186/2042-5783-1-3
520 Glasser, N. R., Kern, S. E., & Newman, D. K. (2014). Phenazine redox cycling enhances
521 anaerobic survival in *Pseudomonas aeruginosa* by facilitating generation of ATP and a
522 proton-motive force. Molecular Microbiology, 92(2), 399.
523 https://doi.org/10.1111/MMI.12566
524 Güell, M., E, Y., M, L.-S., & L, S. (2011). Bacterial transcriptomics: what is beyond the RNA
525 horiz-ome? Nature Reviews. Microbiology, 9(9), 658–669.
526 https://doi.org/10.1038/NRMICRO2620
527 Hoffman, L. R., Richardson, A. R., Houston, L. S., Kulasekara, H. D., & Martens-Habbena, W.
528 (2010). Nutrient availability as a mechanism for selection of antibiotic tolerant
529 *Pseudomonas aeruginosa* within the CF airway. PLoS Pathog, 6(1), 1000712.
530 https://doi.org/10.1371/journal.ppat.1000712
531 Hong, W. X., Hu, M. S., Esquivel, M., Liang, G. Y., Rennert, R. C., McArdle, A., Paik, K. J.,
532 Duscher, D., Gurtner, G. C., Lorenz, H. P., & Longaker, M. T. (2014). The role of
533 hypoxia-inducible factor in wound healing. Advances in Wound Care, 3(5), 390–399.
534 https://doi.org/10.1089/wound.2013.0520
535 James, G. A., Ge Zhao, A., Usui, M., Underwood, R. A., Nguyen, H., Beyenal, H., … Stewart,
536 P. S. (2016). Microsensor and transcriptomic signatures of oxygen depletion in

bioRxiv preprint doi: https://doi.org/10.1101/2022.03.11.484052; this version posted March 12, 2022. The copyright holder for this preprint (which was not certified by peer review) is the author/funder, who has granted bioRxiv a license to display the preprint in perpetuity. It is made available under aCC-BY-NC-ND 4.0 International license.

537 biofilms associated with chronic wounds. Wound Repair and Regeneration, 24(2),
538 373–383. https://doi.org/10.1111/wrr.12401
539 Jo, J., Price-Whelan, A., & Dietrich, L. E. P. (2014). An Aerobic Exercise : Defining the Roles
540 of *Pseudomonas aeruginosa* Terminal Oxidases, 196(24), 4203–4205.
541 https://doi.org/10.1128/JB.02336-14
542 Jo, J., Cortez, K. L., Cornell, W. C., Price-Whelan, A., & Dietrich, L. E. P. (2017). An orphan
543 cbb3-type cytochrome oxidase subunit supports *Pseudomonas aeruginosa* biofilm
544 growth and virulence. ELife, 6. https://doi.org/10.7554/ELIFE.30205
545 Kolpen, M., Kühl, M., Bjarnsholt, T., Moser, C., Hansen, C. R., Liengaard, L., … Jensen, P. Ø.
546 (2014). Nitrous oxide production in sputum from cystic fibrosis patients with chronic
547 *Pseudomonas aeruginosa* lung infection. PLoS ONE, 9(1), e84353.
548 https://doi.org/10.1371/journal.pone.0084353
549 Kopf, M., C, S., & SP, N. (2015). The development and function of lung-resident
550 macrophages and dendritic cells. Nature Immunology, 16(1), 36–44.
551 https://doi.org/10.1038/NI.3052
552 Kuchina, A., Brettner, L. M., Paleologu, L., Roco, C. M., Rosenberg, A. B., Carignano, A., …
553 Seelig, G. (2021). Microbial single-cell RNA sequencing by split-pool barcoding.
554 Science, 371(6531).
555 https://doi.org/10.1126/SCIENCE.ABA5257/SUPPL_FILE/ABA5257_TABLE_S4.CSV
556 Kuroki, M., Y, I., M, I., & H, A. (2014). Fine-tuned regulation of the dissimilatory nitrite
557 reductase gene by oxygen and nitric oxide in *Pseudomonas aeruginosa.*
558 Environmental Microbiology Reports, 6(6), 792–801. https://doi.org/10.1111/1758-
559 2229.12212
560 Kuypers, M. M. M., Marchant, H. K., & Kartal, B. (2018). The microbial nitrogen-cycling
561 network. Nature Reviews Microbiology 2018 16:5, 16(5), 263–276.
562 https://doi.org/10.1038/nrmicro.2018.9
563 Line, L., Alhede, M., Kolpen, M., KÃ¼hl, M., Ciofu, O., Bjarnsholt, T., … Jensen, P. Ã. (2014).
564 Physiological levels of nitrate support anoxic growth by denitrification of
565 *Pseudomonas aeruginosa* at growth rates reported in cystic fibrosis lungs and

bioRxiv preprint doi: https://doi.org/10.1101/2022.03.11.484052; this version posted March 12, 2022. The copyright holder for this preprint (which was not certified by peer review) is the author/funder, who has granted bioRxiv a license to display the preprint in perpetuity. It is made available under aCC-BY-NC-ND 4.0 International license.

566 sputum. Frontiers in Microbiology, 5(OCT), 554.
567 https://doi.org/10.3389/fmicb.2014.00554
568 Marras, S. A. E., Bushkin, Y., & Tyagi, S. (2019). High-fidelity amplified FISH for the
569 detection and allelic discrimination of single mRNA molecules. Proceedings of the
570 National Academy of Sciences, 116(28), 13921–13926.
571 https://doi.org/10.1073/PNAS.1814463116
572 Martins, B., & JC, L. (2015). Microbial individuality: how single-cell heterogeneity enables
573 population level strategies. Current Opinion in Microbiology, 24, 104–112.
574 https://doi.org/10.1016/J.MIB.2015.01.003
575 Michielsm, JE, B, V. den B., N, V., & J, M. (2016). Molecular mechanisms and clinical
576 implications of bacterial persistence. Drug Resistance Updates : Reviews and
577 Commentaries in Antimicrobial and Anticancer Chemotherapy, 29, 76–89.
578 https://doi.org/10.1016/J.DRUP.2016.10.002
579 Nikolakakis, K., Lehnert, E., McFall-Ngai, M. J., & Ruby, E. G. (2015). Use of hybridization
580 chain reaction-fluorescent in situ hybridization to track gene expression by both
581 partners during initiation of symbiosis. Applied and Environmental Microbiology,
582 81(14), 4728–4735. https://doi.org/10.1128/AEM.00890-15
583 Palmer, K. L., Brown, S. A., & Whiteley, M. (2007). Membrane-bound nitrate reductase is
584 required for anaerobic growth in cystic fibrosis sputum. Journal of Bacteriology,
585 189(12), 4449–4455. https://doi.org/10.1128/JB.00162-07
586 Smriga, S., Ciccarese, D. & Babbin, A.R. Denitrifying bacteria respond to and shape
587 microscale gradients within particulate matrices. Commun Biol 4, 570 (2021).
588 https://doi.org/10.1038/s42003-021-02102-4
589 Smits, W., OP, K., & JW, V. (2006). Phenotypic variation in bacteria: the role of feedback
590 regulation. Nature Reviews. Microbiology, 4(4), 259–271.
591 https://doi.org/10.1038/NRMICRO1381
592 Sparacino-Watkins, C., Stolz, J. F., & Basu, P. (2014). Nitrate and periplasmic nitrate
593 reductases. Chemical Society Reviews, 43(2), 676–706.
594 https://doi.org/10.1039/c3cs60249d

bioRxiv preprint doi: https://doi.org/10.1101/2022.03.11.484052; this version posted March 12, 2022. The copyright holder for this preprint (which was not certified by peer review) is the author/funder, who has granted bioRxiv a license to display the preprint in perpetuity. It is made available under aCC-BY-NC-ND 4.0 International license.

595 Speicher, M. R., & Carter, N. P. (2005). The new cytogenetics: Blurring the boundaries with
596 molecular biology. Nature Reviews Genetics, 6(10), 782–792.
597 https://doi.org/10.1038/nrg1692
598 Spero, M. A., & Newman, D. K. (2018). Chlorate specifically targets oxidant-starved,
599 antibiotic-tolerant populations of pseudomonas aeruginosa biofilms. MBio, 9(5).
600 https://doi.org/10.1128/mBio.01400-18
601 Spiro, S. (2012). Nitrous oxide production and consumption: Regulation of gene expression
602 by gas sensitive transcription factors. Philosophical Transactions of the Royal Society
603 B: Biological Sciences. Royal Society. https://doi.org/10.1098/rstb.2011.0309
604 Stewart, P. S. (2003). Diffusion in biofilms. Journal of Bacteriology, 185(5), 1485–1491.
605 https://doi.org/10.1128/JB.185.5.1485-1491.2003/ASSET/6D19778E-CAF8-421A-
606 8618-E4F040153A00/ASSETS/GRAPHIC/JB0530965002.JPEG
607 Thattai, M., & A, van O. (2004). Stochastic gene expression in fluctuating environments.
608 Genetics, 167(1), 523–530. https://doi.org/10.1534/GENETICS.167.1.523
609 Toussaint, B., Delic-Attree, I., R, D. S. D., L, D., M, V., & PM, V. (1993). Purification of the
610 integration host factor homolog of *Rhodobacter capsulatus*: cloning and sequencing
611 of the *hip* gene, which encodes the beta subunit. Journal of Bacteriology, 175(20),
612 6499–6504. https://doi.org/10.1128/JB.175.20.6499-6504.1993
613 Trivedi, V., Choi, H. M. T., Fraser, S. E., & Pierce, N. A. (2018). Multidimensional
614 quantitative analysis of mRNA expression within intact vertebrate embryos.
615 Development (Cambridge), 145(1). https://doi.org/10.1242/dev.156869
616 Turner, K. H., Everett, J., Trivedi, U., Rumbaugh, K. P., & Whiteley, M. (2014). Requirements
617 for *Pseudomonas aeruginosa* acute burn and chronic surgical wound infection. PLoS
618 Genetics, 10(7), e1004518. https://doi.org/10.1371/journal.pgen.1004518
619 Vázquez-Torres, A., & Bäumler, A. (2016). Nitrate, nitrite and nitric oxide reductases: from
620 the last universal common ancestor to modern bacterial pathogens. Current Opinion
621 in Microbiology, 29, 1–8. https://doi.org/10.1016/J.MIB.2015.09.002
622 Walters, M. C., Roe, F., Bugnicourt, A., Franklin, M. J., & Stewart, P. S. (2003). Contributions
623 of antibiotic penetration, oxygen limitation, and low metabolic activity to tolerance of

bioRxiv preprint doi: https://doi.org/10.1101/2022.03.11.484052; this version posted March 12, 2022. The copyright holder for this preprint (which was not certified by peer review) is the author/funder, who has granted bioRxiv a license to display the preprint in perpetuity. It is made available under aCC-BY-NC-ND 4.0 International license.

624 *Pseudomonas aeruginosa* biofilms to ciprofloxacin and tobramycin. Antimicrobial
625 Agents and Chemotherapy, 47(1), 317–323. https://doi.org/10.1128/AAC.47.1.317-
626 323.2003
627 Wilbert, S.A., and Newman, D.K. (2021). The double-edged role of nitric oxide drives
628 predictable microbial community organization according to the microenvironment.
629 bioRxiv 2021.12.09.472001.
630 Williams, D. R., Rowe, J. J., Romero, P., & Eagon, R. G. (1978). Denitrifying *Pseudomonas*
631 *aeruginosa*: Some parameters of growth and active transport. Applied and
632 Environmental Microbiology, 36(2), 257–263. https://doi.org/10.1128/aem.36.2.257-
633 263.1978
634 Xiao, Y., Bowen, C. H., Liu, D., & Zhang, F. (2016). Exploiting nongenetic cell-to-cell
635 variation for enhanced biosynthesis. Nature Chemical Biology 2016 12:5, 12(5), 339–
636 344. https://doi.org/10.1038/nchembio.2046
637 Zhao, G., ML, U., SI, L., GA, J., PS, S., P, F., & JE, O. (2013). Biofilms and Inflammation in
638 Chronic Wounds. Advances in Wound Care, 2(7), 389–399.
639 https://doi.org/10.1089/WOUND.2012.0381
640 Zumft, W. G. (1997). Cell biology and molecular basis of denitrification. Microbiology and
641 Molecular Biology Reviews : MMBR, 61(4), 533–616.
642 https://doi.org/10.1128/.61.4.533-616.1997
643

bioRxiv preprint doi: https://doi.org/10.1101/2022.03.11.484052; this version posted March 12, 2022. The copyright holder for this preprint (which was not certified by peer review) is the author/funder, who has granted bioRxiv a license to display the preprint in perpetuity. It is made available under aCC-BY-NC-ND 4.0 International license.

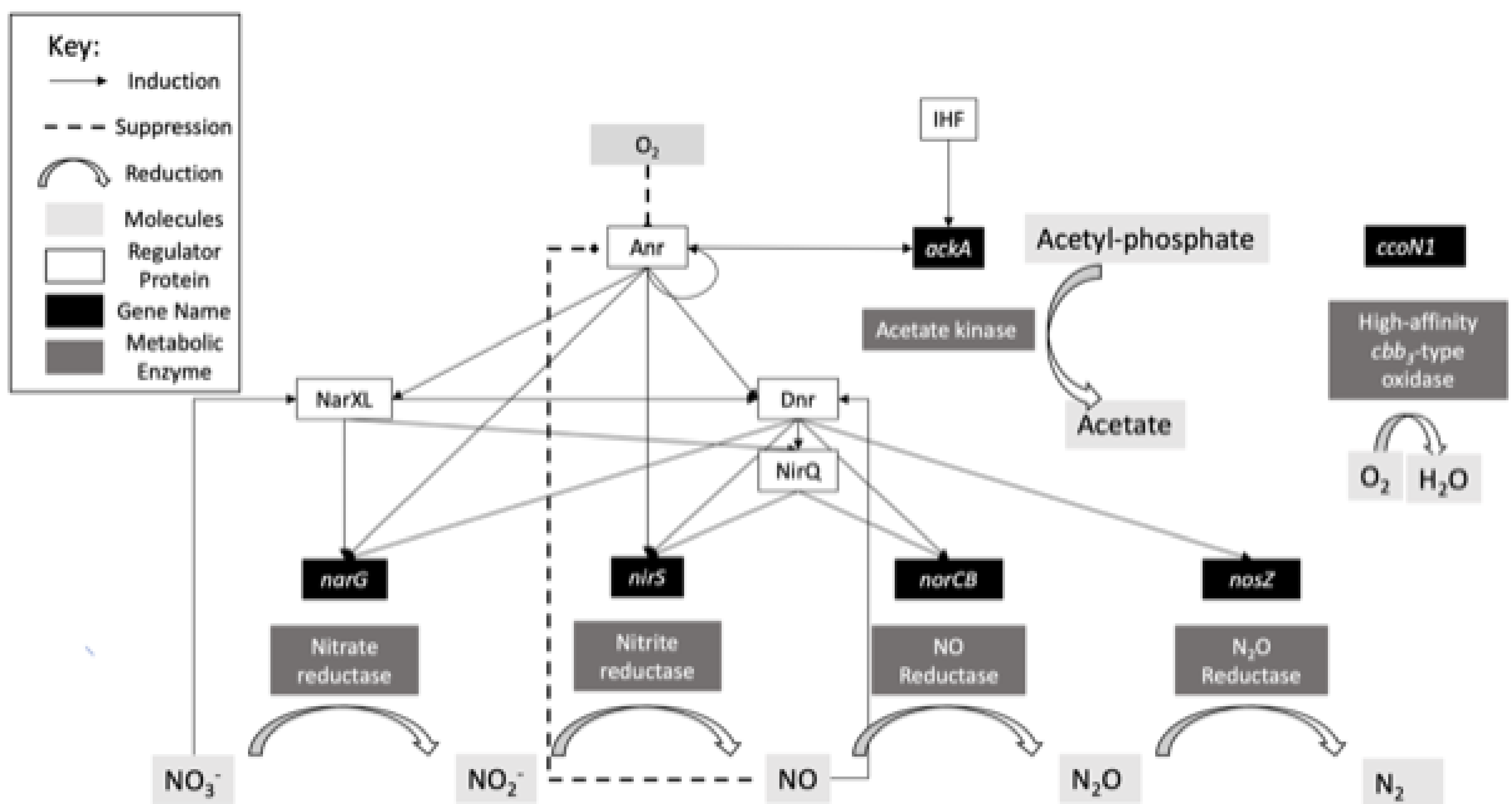

bioRxiv preprint doi: https://doi.org/10.1101/2022.03.11.484052; this version posted March 12, 2022. The copyright holder for this preprint (which was not certified by peer review) is the author/funder, who has granted bioRxiv a license to display the preprint in perpetuity. It is made available under aCC-BY-NC-ND 4.0 International license.

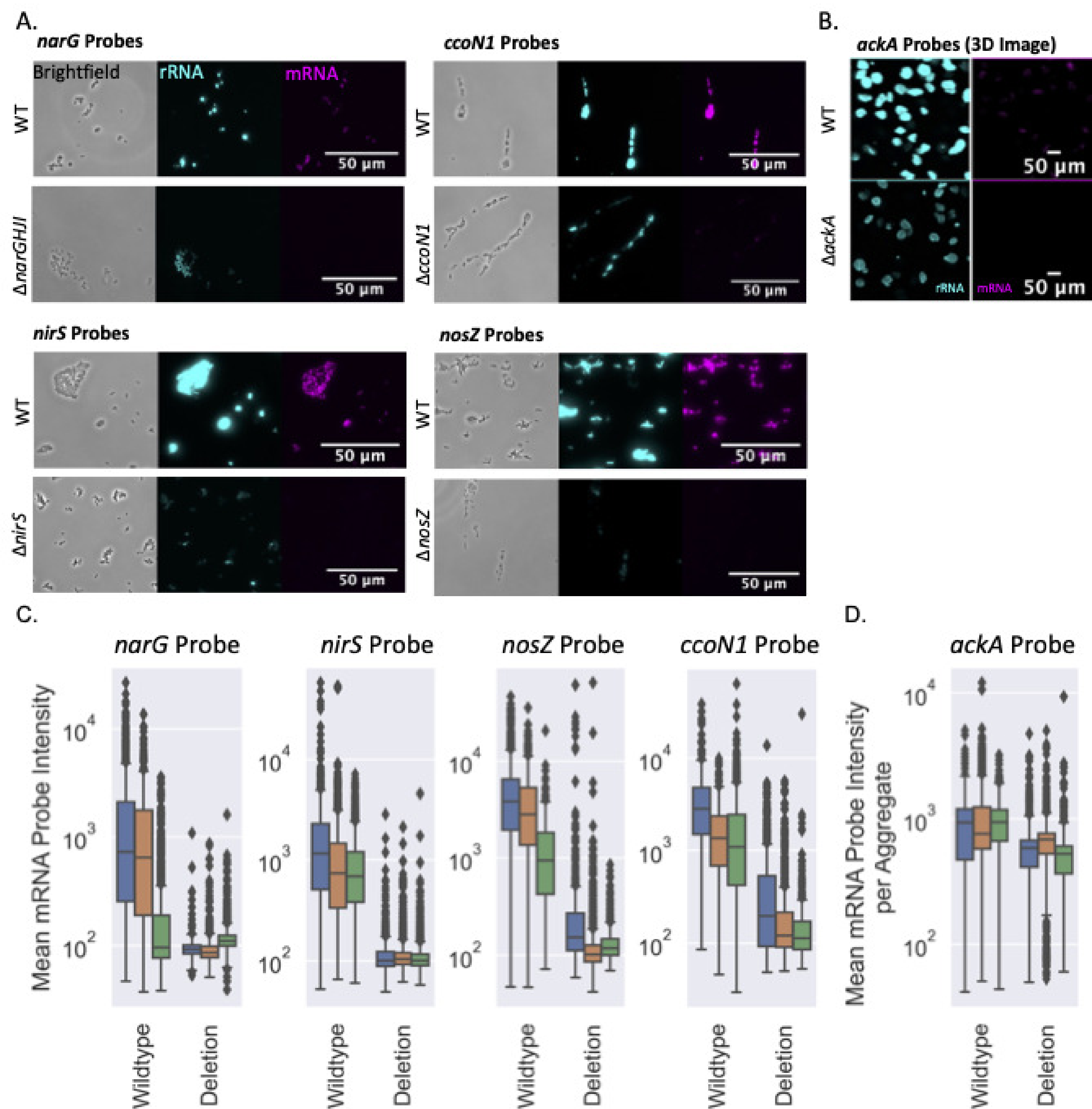

bioRxiv preprint doi: https://doi.org/10.1101/2022.03.11.484052; this version posted March 12, 2022. The copyright holder for this preprint (which was not certified by peer review) is the author/funder, who has granted bioRxiv a license to display the preprint in perpetuity. It is made available under aCC-BY-NC-ND 4.0 International license.

A

Depth (μm)
O2 (μmol/L)

B

ccoN1 *ackA* *narG* *nirS* *nosZ*

Depth
0-50 μm
50-100 μm
100-150 μm
150-200 μm
200-250 μm
250-300 μm
300-350 μm
350-400 μm
400-450 μm
450-500 μm

Merge rRNA mRNA
200 μm

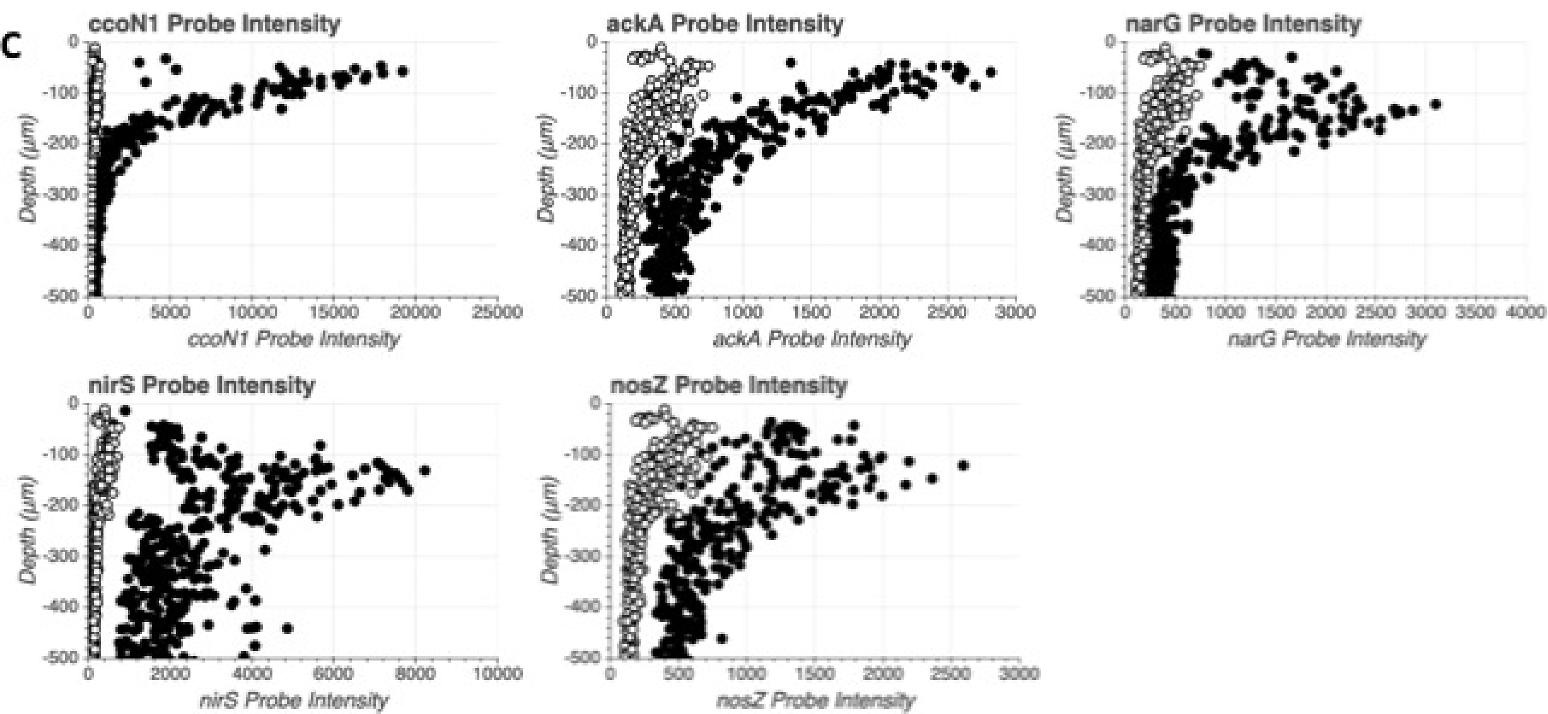

bioRxiv preprint doi: https://doi.org/10.1101/2022.03.11.484052; this version posted March 12, 2022. The copyright holder for this preprint (which was not certified by peer review) is the author/funder, who has granted bioRxiv a license to display the preprint in perpetuity. It is made available under aCC-BY-NC-ND 4.0 International license.